Toward Combining Graphene and QDs: Assembling CdTe QDs to Exfoliated Graphite and Nanographene in Water

Georgios Katsukis, Jenny Malig, Christian Schulz-Drost, Susanne Leubner, Norbert Jux, and Dirk M. Guldi*

Department of Chemistry and Pharmacy & Interdisciplinary Center for Molecular Materials, Friedrich-Alexander-Universität Erlangen-Nürnberg, Egerlandstraße 3, 91058 Erlangen, Germany

ABSTRACT

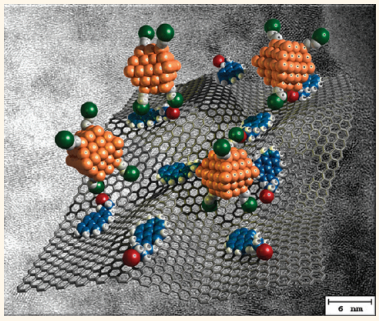

Herein, we report for the first time on a full-fledged investigation of water-soluble CdTe quantum dots (QD) that are immobilized onto exfoliated graphite (EG) and/or nanographene (NG). Particular emphasis was placed on a top-down preparation of stable aqueous dispersions—starting from natural graphite rather than graphene oxide—while preserving the intrinsic properties of graphene. To this end, we circumvented the harsh conditions commonly employed for the pre-exfoliation (*i.e.*, Hummers method). First, a hydrophobic—hydrophobic/$\pi-\pi$ stacking motif was tested between EG and pyrene, to which QDs are covalently attached (QD-pyrene). Second, we employed the combination of hydrophobic—hydrophobic/$\pi-\pi$ stacking and electrostatic interactions to build up hierarchical structures composed of NG, positively charged pyrene (pyrene$^+$), and negatively charged QDs. The novel nanohybrids—QD-pyrene/EG and QD/pyrene$^+$/NG—were characterized with specific emphasis on electron-transfer chemistry. In fact, both assays provide kinetic and spectroscopic evidence that support electron transfer dynamics that vary, however, between EG and NG as a reflection of the different degree of graphite exfoliation.

KEYWORDS: nanographene · exfoliated graphite · CdTe quantum dots · time-resolved spectroscopy · electron transfer

Due to its outstanding mechanical and electronic properties, graphene has emerged as the unrivaled candidate in the emerging field of nanotechnology.[1] The extraordinary potentials of graphene are keenly tested in post-silicon nanoelectronics,[2] since it might offer the answer to the fast approaching physical limits of currently used materials. For instance, graphene-based transparent conducting electrodes compete with the standard of industry, namely, indium tin oxide (ITO).[3,4] Here, the full potential use of graphene requires, however, doping by electron donors and/or electron acceptors.[5−7]

So far, major breakthroughs—including the fabrication of single-layer graphene—came from substrate-related preparation procedures.[3,8] An alternative approach involves the formation of graphene oxide under highly oxidizing conditions, which has emerged as the most common strategy to produce chemically modified graphene.[9] In light of the disrupted sp^2-networks, graphene oxide lacks the electronic quality of pristine graphene. To this end, restoring the sp^2-network by chemical reduction becomes a crucial step. Notably, the reduction leads irreversibly to partially amorphous carbon.[10,11] As a matter of fact, the resulting reduced graphene oxide exhibits features that are similar but not identical when compared to that of pristine graphene.

More recently, milder wet chemical approaches toward high-quality graphene flakes encompass the use of graphite as a starting material, which is mechanically separated into individual atomic planes by means of ultrasonic treatment in solution.[5] Notably, such a wet chemical approach cannot be performed without any chemical modification/functionalization or without subsequent stabilization of the resulting graphene layers.[12] A common denominator of these methods is a suitable amphiphilic intercalator and/or solvent that guarantees the efficient exfoliation. The intercalator should be multifunctional; desirable features include among many others photo and redox activity. Considering the aforementioned, we developed a solution-based approach to realize a preparation of hybrid materials, which enabled combining few-layer graphene with metallophthalocyanines in organic solvents. Since metallophthalocyanines are photo and redox active, it comes as no surprise that the resulting hybrid materials were

* Address correspondence to guldi@chemie.uni-erlangen.de.

Received for review October 8, 2011 and accepted February 20, 2012.

Published online February 21, 2012
10.1021/nn204700z

successfully incorporated from THF suspensions as an active layer into photoelectrochemical cells.[13]

Owing to the outstanding features of CdTe quantum dots (QDs), namely, sizable absorptions throughout the visible and range, narrow, and widely tunable photoluminescence along with high photostability, their close resemblance to bulk inorganic semiconductors has motivated intense studies and has led to the realization of numerous applications.[14−17] Recently, synthetic strategies for integrating single QD systems—TiO_2, ZnO, Au, Pt, Pd, CdS, CdTe—onto graphene oxide and reduced graphene oxide have been developed for potential use in catalysis, light energy conversion, and sensors.[18−38] Future scientific and technological breakthroughs will depend, in large, on key achievements such as applying the approach of electronic coupling of these crystalline QDs to better performing, multifunctional materials such as pristine graphene rather than graphene oxide/reduced graphene oxide, which require a number of time-consuming and challenging steps to reach synthetically the same goals. Of particular importance are in this context lattice defects/dopant that are present in graphene oxide/reduced graphene oxide, which impact carrier mobility and electronic transitions.

Nevertheless, the need for a gentle preparation of graphene-based hybrid materials is omnipresent, in which an environmentally friendly and cheap solvent such as water and natural graphite as starting material are employed. This would, in turn, enable the noncovalent immobilization of inorganic quantum dots onto the honeycomb lattice by means of intermolecular noncovalent forces and thus the fine-tuning of the electronic coupling as an important requisite for energy and electron-transfer reactions. In contrast to recent work on inorganic quantum dots/graphenoid hybrids, in which the focus was directed on graphene oxide that was subsequently reduced with hydrazine or CVD-grown graphene, to which QDs (*i.e.*, CdS or CdTe) were attached, our concept is novel.[18−31]

RESULTS AND DISCUSSION

In light of recent accomplishments of interfacing CdTe QDs with fullerenes and/or carbon nanotubes[39−42] we have pursued in this study two different strategies, namely, as outlined in Scheme 1, a direct and a sequential approach, toward the integration of QDs onto the basal plane of graphene in water rather than graphene oxide and/or reduced graphene oxide. First, a hydrophobic−hydrophobic/$\pi-\pi$ stacking motif was tested between exfoliated graphite (EG) and pyrene, to which QDs are covalently attached: QD-pyrene. Second, we employed the combination of hydrophobic−hydrophobic/$\pi-\pi$ stacking and electrostatic interactions to built up hierarchical structures composed of nanographene (NG), positively charged pyrene (*i.e.*, trimethyl(2-oxo-2-pyren-1-ylethyl)ammonium bromide) (pyrene$^+$), and negatively charged thioglycolic acid (TGA)/2-mercaptoethanesulfonate (MESNA) costabilized

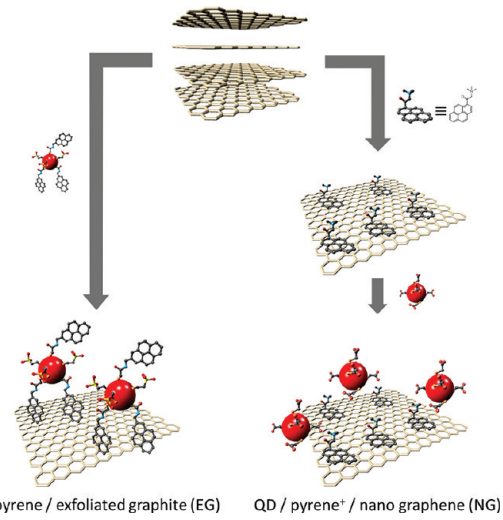

Scheme 1. Schematic representation of a direct and a sequential approach, that is, QD-pyrene/EG and QD/pyrene$^+$/NG, on the left and on the right, respectively, toward combining graphene and QDs.

QDs (Scheme 1). Importantly, the interactions between the individual components are essential to gain full control over dispersibility, solubility, and functionality of the resulting hybrids.

Interfacing QD-Pyrene with Exfoliated Graphite. Our first "direct" approach is based entirely on hydrophobic−hydrophobic/$\pi-\pi$ stacking interactions between the basal plane of graphene and QDs. Rendering TGA/MESNA-capped QDs, however, susceptible to hydrophobic forces required the covalent attachment of 1-pyrenemethylamine; for details see the Methods section. The latter was corroborated by IR spectroscopy—see Figure S1 in the Supporting Information—where QDs show characteristic IR absorption features in the region between 3650 and 3000 cm^{-1} (ν(OH), H_2O), next to the asymmetric stretching vibration $\nu_{as}(COO^-)$ at 1576 cm^{-1}, and the deformation vibration δ(OH) at 1380 cm^{-1}. The absence of S−H vibrations at 2560−2580 cm^{-1} points to the formation of sulfur−QD bonds. Importantly, the carboxylic acid centered OH stretch band at 3412 cm^{-1} is converted into a N−H stretch band at 3355 cm^{-1} as part of CO−NH−R. Additionally, the C═O stretching and the N−H bending vibrations at 1638 and 1563 cm^{-1}, respectively, provide additional evidence for a successful peptide condensation.

Initially, we performed titrations with pre-exfoliated graphite and QD-pyrene in a mixture of water and DMSO (20:1 v/v). These were performed by ultrasonicating natural graphite in DMSO for 45 min to pre-exfoliate graphite and adding different amounts of this dispersion into a QD-pyrene suspension with a concentration of 0.013 mM. Throughout these titration experiments, both the pyrene-centered (*i.e.*, 264, 275, 325, and 341 nm) and the QD-centered (*i.e.*, excitonic

absorption in the range from 500 to 600 nm) absorptions are discernible. At first glance, they appear as simple superimpositions regardless of the specific concentrations. When turning, however, to the band gap emission of QDs at 578 nm, we noted that the corrected emission spectra (*i.e.*, corrected for the absorption differences arising at the excitation wavelength) give rise to a 4 nm red shift. Such observations resemble a recent report, in which QD-pyrene was immobilized successfully onto the surface of single-wall carbon nanotubes (Figure S2 in the Supporting Information).[41]

The aforementioned let us process QD-pyrene and exfoliated graphite from pure water. In this context, special care was taken to avoid any sonication steps at all, which contrast previous work on exfoliating graphite. The latter is seen to deteriorate QDs within a time window of 30 s.[41] Here, the intrinsic band gap emission was monitored in the presence and absence of exfoliated graphite. Thus, a typical workup procedure comprised QD-pyrene dispersions, to which 0.4 mg/mL of natural graphite was added, that were stirred for three days and kept overnight without stirring, and the supernatant was separated.

Next, we investigated the resulting QD-pyrene/exfoliated graphite system by means of Raman spectroscopy on a Si wafer. The starting material, namely, graphite, gave rise to its typical Raman peaks upon 532 nm excitation; see Figure S3 in the Supporting Information. In particular, the relatively weak D-band at 1350 cm^{-1} implies a low defect density of the starting material and is consistent with the presence of G- and 2D-bands at 1583 and 2716 cm^{-1} with its shoulder at 2680 cm^{-1}, respectively.

As a typical feature of pristine graphitic materials, the 2D-band consists of at least two visible components. The exfoliated and the QD-functionalized graphite exhibits all of the typical graphenoid-centered Raman bands, namely, D-, G-, and 2D-bands, when photoexcited at 532 nm.[43] Most importantly, the 2D-band is still accompanied by a shoulder at 2708 cm^{-1}, is unsymmetrical, and is deconvoluted into a superposition of two Lorentzian components with full widths at half-maxima (fwhm) of 70 and 39 cm^{-1} and a 2D/G ratio of 1:3 for QD-pyrene/exfoliated graphite, Figure 1. In comparison to the pristine graphite with fwhm values of 53 and 36 cm^{-1} for a bi-Lorentzian fit and a 2D/G ratio of 1:2, we reach the conclusion that we are dealing with multilayer graphene and, thus, refer to exfoliated graphite (EG) rather than nanographene (NG), *vide infra*.

Along the same lines, microscopy by means of transmission electron microscopy reveals that exfoliation is far from being quantitative. In particular, the coexistence of few-layer graphene and multilayer graphene is clearly discernible in the HR-TEM images, Figure 2. We attribute this observation to the

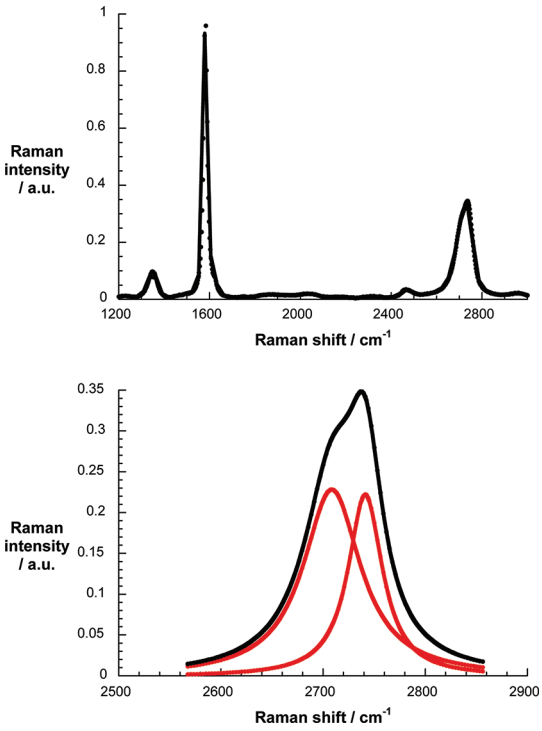

Figure 1. (Top) Raman spectrum of QD-pyrene/EG upon laser excitation at 532 nm drop-coated onto a silicon oxide wafer (300 nm). (Bottom) 2D Raman peak (black spectrum) and its bi-Lorentzian fit (red spectra).

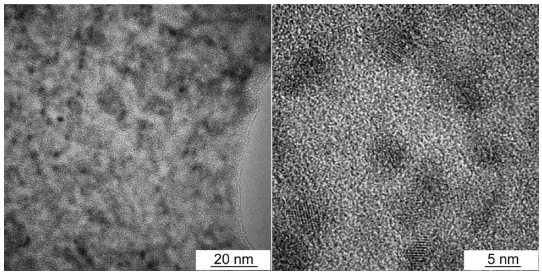

Figure 2. HR-TEM images of QD-pyrene/EG with different magnifications on holey carbon-coated copper grids.

insufficient means of QD-pyrene to penetrate between the individual graphene layers in graphite and reduce the hydrophobic interactions of the graphitic surface with water in the absence of ultrasonication. More important are, however, the insights that the HR-TEM images provide into the immobilization of QD-pyrene onto EG that possess flake sizes from 0.27 up to 12.7 μm^2. Representative images suggest the close packing of QDs that are successfully immobilized onto EG. Importantly, we could not identify regions where only QD-pyrene—in the form of either individual QDs or agglomerates of QDs—appears. By the same token, we could not find any structural differences or destructions of spherical-shaped QD-pyrene (*i.e.*, TeO_2) with a mean size of around 3 nm. The (220) lattice planes of cubic zinc blende QDs are undoubtedly visible in the HR-TEM images, pointing to the high crystallinity of QDs even upon immobilization onto EG.

Next, we compared the band gap emission in QD-pyrene and QD-pyrene/EG with suspensions that exhibit absorbances of 0.09 and 0.17 at the 420 nm excitation wavelength, respectively. In QD-pyrene/EG the excitonic band gap absorption in the range from 500 to 600 nm is superimposed onto features that correspond to EG absorptions and light scattering. Still, the QD emission is quenched in QD-pyrene/EG by a factor of 5 and slightly shifted to the blue (*i.e.*, from 578 to 573 nm) relative to QD-pyrene, Figure 3. Such a trend reflects a change in electronic coupling that predominates initially between QD and pyrene and that transforms into coupling between pyrene and EG. To confirm that the QD size has not been impacted by the workup procedure, especially in light of their susceptibility to physical damage or to agglomeration, corresponding excitation spectra were taken, Figure S4 in the Supporting Information. With particular focus on the 573 nm emission maximum, an excitation spectrum evolved that revealed the excitonic band in the range from 500 to 600 nm and is, thus, virtually identical to what has been seen in the absence of EG. From the latter we infer the lack of significant agglomeration.

Complementary time-resolved emission experiments with 467 nm as excitation wavelength and 573 nm as emission wavelength further corroborated the quenching seen in the steady-state emission experiments. For QD-pyrene/EG, the lifetimes of 0.6 (25%), 4.3 (52%), and 21.6 ns (23%) are notably shorter than 1.2 (25%), 6.6 (55%), and 32.9 ns (20%), as they were derived for QD-pyrene in the absence of EG, Figure S5 in the Supporting Information.

Finally, we turned to transient absorption measurements. In the case of QD-pyrene, the characteristic features of QDs evolve upon 387 nm excitation, Figure S6 in the Supporting Information. The latter are dominated in the visible range by bleaching of the QD band gap transition. The bleaching is centered at 534 nm for just QD-pyrene, which is nearly identical to what has been seen for QD.[41] Multiwavelength analyses of the transient decays throughout the entire visible range afforded three lifetimes for QD-pyrene, namely, 5.8, 48, and >7800 ps with relative weights of 73%, 18%, and 9%, respectively. Notably, the two short-lived components relate to filling shallow and deep traps.[44] During such trap fillings the differential absorption changes transform into maxima at 463 and 615 nm as well as a minimum at 541 nm. In the near-infrared, which features a broad QD absorption centered at 1098 nm, the main component (*i.e.*, short-lived hole intraband absorption)[45,46] is seen to decay in 3.7 ps and to afford a new maximum at 930 nm. Once more at the end of the femtosecond time-scale (*i.e.*, 7800 ps) a long-lived excited state remains. In QD-pyrene/EG, the bleaching minimizes at 528 nm, which implies a blue-shift similar to that seen in the emission experiments, namely,

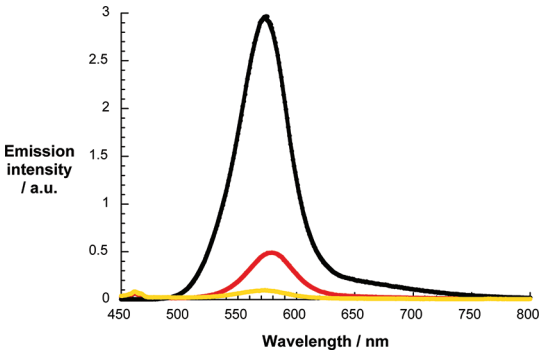

Figure 3. Emission spectra upon 420 nm excitation of QD (black spectrum), QD-pyrene (red spectrum), and QD-pyrene/EG (orange spectrum) in aqueous dispersion that exhibit optical absorbances of 0.09 for QD and QD-pyrene and 0.17 for QD-pyrene/EG at the 420 nm excitation wavelength.

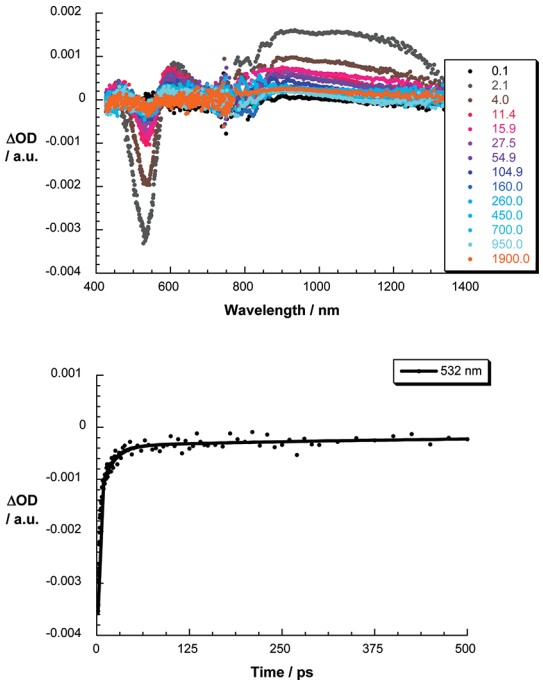

Figure 4. (Top) Differential absorption spectra (visible and near-infrared) obtained upon femtosecond flash photolysis (387 nm, 200 nJ) of QD-pyrene/EG in water with several time delays between 0.1 and 1900 ps at room temperature; see legend for details. (Bottom) Time–absorption profile of the spectra shown above at 532 nm.

QD-pyrene *versus* QD-pyrene/EG, Figure 4. Note that in these experiments a rather broad distribution in terms of graphene layers and in terms of flake size are investigated. Nevertheless, two short-lived components emerge with values that are significantly shorter than in QD-pyrene, namely, 3.5 (75%) and 29 ps (16%). Compare them to 5.5 (73%) and 48 ps (18%), *vide supra*. During these decays features develop that include 467/614 nm maxima and a 533 nm minimum. At time delays of 100 ps and beyond no further changes were noted in the differential absorption spectra. The near-infrared lacks the graphenoid-centered bleaching due

to an insufficient exfoliation of graphite and the superimposition on the QD-pyrene hole-intraband absorption.

Interfacing QDs with Nanographene. In light of the partial success in graphite exfoliation we turned to the second "sequential" approach, which involved the use of hydrophobic−hydrophobic/$\pi-\pi$ stacking interactions between trimethyl(2-oxo-2-pyrene-1-ylethyl)ammonium bromide[47] (pyrene$^+$) and graphene followed by electrostatic interactions with TGA/MESNA-capped QDs; for details see the Methods section.

The tendency of pyrene$^+$ to form aggregates in water is particularly helpful for monitoring its successful integration onto the basal plane of graphite and is corroborated by the broad excimer-like emission that sets in at around 10^{-9} M.[48] The latter is accompanied by fluorescence lifetimes of less than 3 ns and fluorescence quantum yields as low as 0.01.[48] In terms of exfoliating graphite an excess of pyrene$^+$ was ultrasonicated in aqueous solution in the presence of natural graphite. To remove free pyrene$^+$, the residue was resuspended, followed by ultrasonication and characterization by means of absorption/emission spectroscopy, *vide infra*. Notable is that the equilibrium between free pyrene$^+$ and immobilized pyrene$^+$ prevents a full and quantitative removal. In steady-state absorptions no particular changes were noted between the two forms: free pyrene$^+$ *versus* immobilized pyrene$^+$. To this end, absorption maxima are always discernible at 232, 288, 367, and 392 nm, Figure S7 in the Supporting Information.

Independent confirmation for the graphite exfoliation was obtained from Raman spectroscopical investigations. In particular, the D-band intensifies during exfoliation. This trend reflects smaller flake sizes and, thus, an increased contribution of double-resonant Raman scattering processes at the edges. The 2D-band transforms into a highly symmetric peak that is redshifted to 2675 cm^{-1} upon excitation at 532 nm with a fwhm of 54 cm^{-1}, Figure 5. A deconvolution into one Lorentzian fit points to monolayer graphene. From the latter we conclude the highly exfoliated character of natural graphite that was employed as starting material. As a matter of fact, we take the outcome of the Raman investigations to use the term nanographene.

Next to Raman experiments, valuable insights into further structural features of the QD/pyrene$^+$/NG system were acquired by HR-TEM (Figure 6) as well as by atomic force microscopy (AFM) (Figure S8 in the Supporting Information) on a carbon-coated copper grid and 300 nm silicon oxide wafer, respectively. HR-TEM experiments reveal well and uniformly dispersed QDs with their (220) lattice planes of cubic zinc blende immobilized on the mono- to few-layer-graphene flakes, which are folded and intertwined on the substrate.[49] In addition, height profiles reveal up to 5−10 nm high flakes.

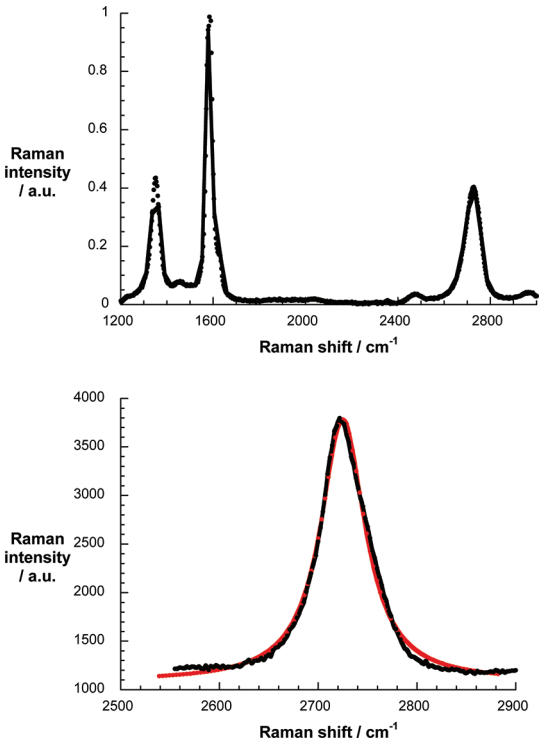

Figure 5. (Top) Raman spectrum of QD/pyrene$^+$/NG upon laser excitation at 532 nm drop-coated onto a silicon oxide wafer (300 nm). (Bottom) 2D Raman peak (black spectrum) and its Lorentzian fit (red spectrum).

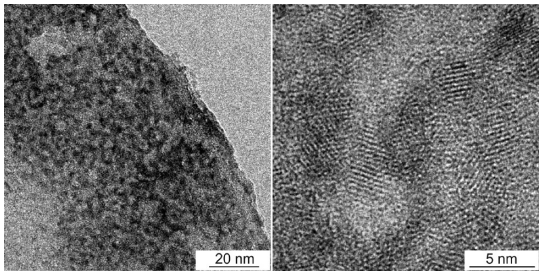

Figure 6. HR-TEM images of QD/pyrene$^+$/NG with different magnifications drop-casted on a carbon-coated copper grid.

When comparing the overall degree of exfoliation seen with QD-pyrene and pyrene$^+$ in water, the interactions of pyrene$^+$ with the graphene lattice are dominated by hydrophobic forces, which are beneficial to afford a maximum degree of graphite exfoliation. Nevertheless, the need for ultrasound treatment is eminent, as it initiates the exfoliation of graphite through taking apart individual graphene layers.

As already mentioned, the absorption features of pyrene$^+$ are not noticeably impacted by the presence of NG, but the emission features are remarkably different. In particular, the interactions with NG convert the excimer-like emission of pyrene$^+$ (*i.e.*, 501 nm maximum) into the monomer-like emission (*i.e.*, 383, 398, and 424 nm maxima), Figure 7. At the end of the transformation, it is only the quenched monomer-like

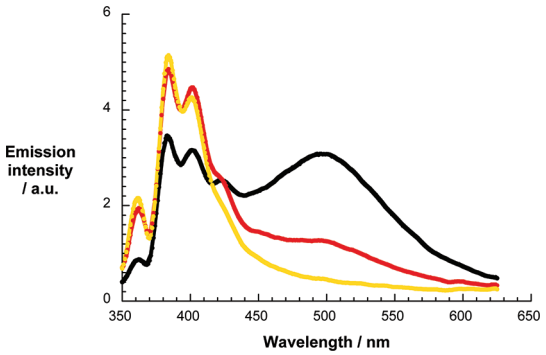

Figure 7. Emission spectra of aqueous dispersions of pyrene$^+$ (0.005 mM) and NG (black spectrum) and after one (red spectrum) and two washing cycles (orange spectrum) that exhibit optical absorbances of 0.90, 0.51, and 0.29, respectively, at the 340 nm excitation wavelength.

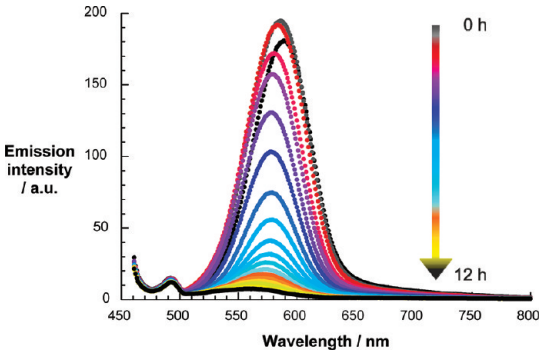

Figure 8. Emission spectra of QD/pyrene$^+$/NG recorded in 30 min intervals upon excitation at 450 nm. See figure legend for details about the progression.

emission that remains detectable. Likewise, the emission lifetimes are impacted with dynamics that are best fitted by triexponential decay functions with lifetimes of 30.9 ns (45%), 6.1 ns (25%), and 1.6 ns (30%) due to free pyrene$^+$ and immobilized pyrene$^+$ on single-layer and/or few-layer graphene, respectively, Figure S9 in the Supporting Information.

Next, titration assays were conducted in the absence of NG. To this end, pyrene$^+$ was titrated with variable amounts of QD and QD was titrated with variable amounts of pyrene$^+$. Common to both sets of titrations is that the absorptions develop as linear superimpositions of both constituents, Figure S8. In fact, the only noticeable difference is a steadily increasing absorption of either QD (*i.e.*, 556 nm) or pyrene$^+$ (*i.e.*, 232, 287, and 366 nm) as they were added, which points out that no significant aggregation takes place, Figure S10 in the Supporting Information. On the contrary, probing the emission of QD or pyrene$^+$ upon excitation at 450 or 340 nm, respectively, had a profound impact, Figure S11 in the Supporting Information. Most importantly, the QD emission band with its peak at 591 nm is quenched upon 450 nm excitation, is red-shifted from 591 to 603 nm, and is not broadened. It should be noted that pyrene$^+$ tends to interact with QDs through electrostatic interactions, from which we conclude that the predominant cause for the emission quenching in QD/pyrene$^+$ is the immobilization of pyrene$^+$ onto the surface of the QDs.[50,51] Important in this context is the AFM/TEM/HR-TEM analysis of QD/pyrene$^+$/NG (*vide supra*), which documents the absence of QD agglomerates. Formation of the latter is known to induce emission quenching of the QDs.[39−42]

Likewise, exciting into the pyrene$^+$-centered features at 340 nm results in a quenched emission. The broad excimer-like emission band is present at 502 nm and partly superimposed onto the QD emission. Implicit is a nonradiative deactivation pathway that involves either a transduction of excited-state energy or an electron transfer. The latter would infer oxidation of QD and reduction of pyrene$^+$, which is, however, on thermodynamic grounds unlikely to happen.

The relative quantum yields were determined by contrasting, for example, the aforementioned experiments with QD/pyrene$^+$ and QD/pyrene$^+$/NG. Following each addition step, the corresponding absorption and fluorescence spectra of the resulting solutions were immediately recorded and compared, Figure S10 *versus* S11 and Figure S12 *versus* S13 in the Supporting Information. In the relationships, that is, emission intensity *versus* concentration of pyrene$^+$, we noted the marked decrease of the emission. In the earlier case the overall quenching is due to interactions between QDs and pyrene$^+$, while in the latter case it is simply due to the interaction of QD and graphene facilitated by pyrene$^+$ in water, which is also reflected in the emission red shift of both systems (*i.e.*, from 591 to 603 nm for QD/pyrene$^+$ and from 591 to 593 nm for QD/pyrene$^+$/NG). Notable are the lower intensities for QD/pyrene$^+$/NG, which, in turn, correlate with lower emission quantum yields. In fact, compared to dispersions of QD/pyrene$^+$, the emission quantum yield of QD/pyrene$^+$/NG was found to be reduced by 26%, Figure S14 in the Supporting Information.

In light of the aforementioned we probed QD and pyrene$^+$/NG under low concentration conditions, that is, 3.25×10^{-7} M QD and 0.5 mg/mL pyrene$^+$/NG. We noticed that the equilibrium between QD and QD/pyrene$^+$/NG is reached after 12 h. The latter is accompanied by a strong emission quenching and a blue shift from 591 to 567 nm (Figure 8), a finding that goes hand in hand with previously published work on single-walled carbon nanotubes.[41]

Such quenching—QD/pyrene$^+$ *versus* QD/pyrene$^+$/NG—is also inferred from time-resolved emission experiments. Under time-resolved conditions (*i.e.*, 403 nm excitation wavelength and 600 nm emission wavelength), the three dominant components 98.2 ns (25%), 20.3 ns (62%), and 5.3 ns (13%) decrease to 21.7 ns (40%), 7.6 ns (50%), and 1.1 ns (10%) in the absence of NG as well as to 45.2 ns (27%), 9.3 ns (49%), and 2.3 ns (24%) in the presence of NG at the

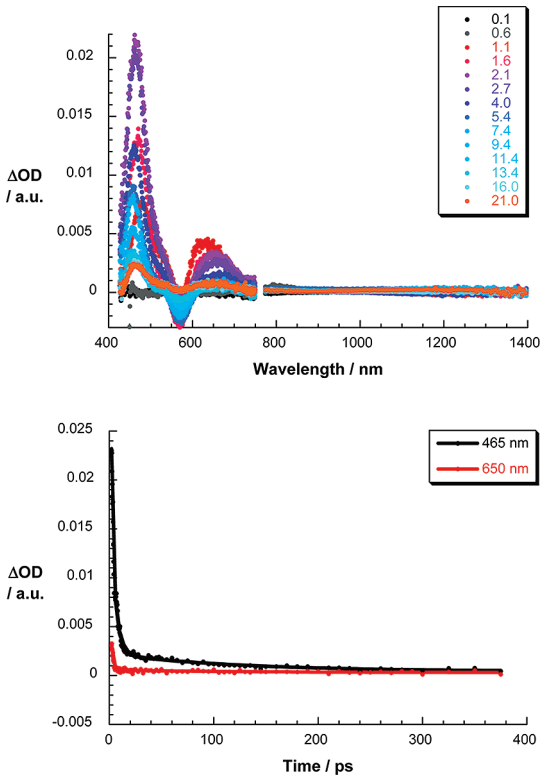

Figure 9. (Top) Differential absorption spectra (visible and near-infrared) obtained upon femtosecond flash photolysis (387 nm) of QD/pyrene^{+} in water with several time delays between 0.1 and 21.0 ps at room temperature; see legend for details. (Bottom) Time−absorption profiles of the spectra shown above at 465 (black profile) and 650 nm (red profile).

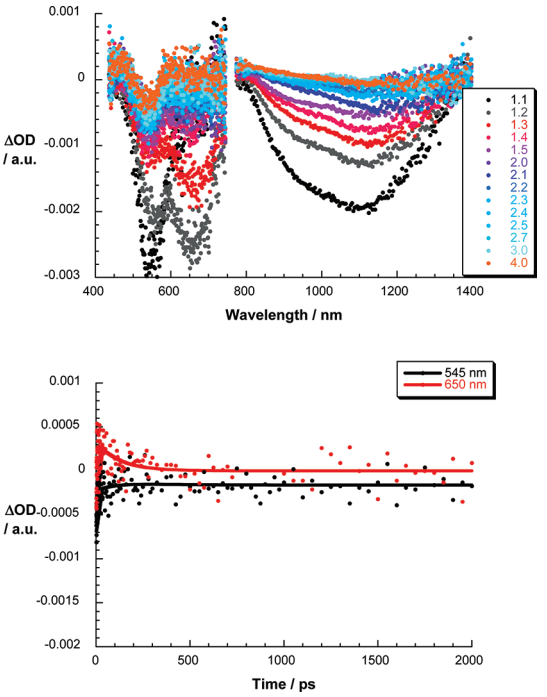

Figure 10. (Top) Differential absorption spectra (visible and near-infrared) obtained upon femtosecond flash photolysis (387 nm) of QD/pyrene^{+}/NG in water with several time delays between 1.1 and 4.0 ps at room temperature; see legend for details. (Bottom) Time−absorption profiles of the spectra shown above at 545 (black profile) and 650 nm (red profile).

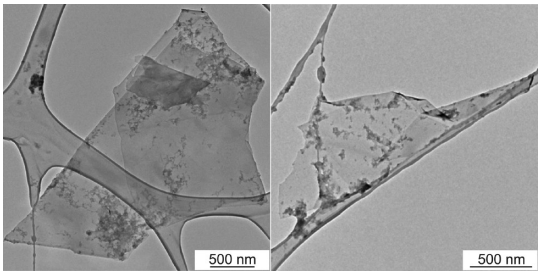

Figure 11. TEM images of QD-pyrene/EG (left) and QD/pyrene^{+}/NG (right) drop-casted on a carbon-coated copper grid.

point of maximum emission quenching, Figure S15 in the Supporting Information.

Finally, we turned to transient absorption measurements. Excitation at 387 nm leads in the case of QD/pyrene^{+} to the characteristic features of QDs, which are slightly red-shifted when compared to those of QDs in the absence of pyrene^{+}, Figure 9. In the visible range, the latter are dominated by bleaching of the QD band gap transition centered at 570 nm and flanked by maxima at 490 and 636 nm. Multiwavelength analyses of the transient decays throughout the entire visible range afforded three QD centered lifetimes, namely, 4.7, 24.0, and 75.0 ps. Please note that a significant portion of the excited-state features remain stable beyond the time-scale of 7800 ps. As aforementioned, the 24 and 75 ps lifetimes relate to filling of shallow and deep traps. Likewise, 387 nm excitation of QD/pyrene^{+}/NG (Figure 10) reveals distinct transient absorption changes. In contrast to the aforementioned experiments with QD-pyrene/EG, the distribution in terms of graphene layers is narrow, while the flake sizes vary appreciably, *vide supra*. The corresponding differential absorption changes feature a minimum that mirror images the QD band gap transition at 541 nm and two maxima at 471 and 648 nm in the visible range. Of particular importance is the observation that a rather broad bleaching dominates the near-infrared range. It reveals a local minimum at 1120 nm and relates to photoexcited NG, in the form of phonons.[52] A global analysis of the differential absorption changes recorded throughout the visible (*i.e.*, QD) and near-infrared (*i.e.*, NG) range brought a lifetime of 10 ps to light. As time progresses, the QD- and NG-centered features undergo marked changes. The QD centered, on one hand, transform into a new maximum at 750 as a reflection of QD oxidation. The NG-centered bleaching, on the other hand, red-shifts from 1120 to 1220 nm. We ascribe this marked red shift—based on the similarity to reduced single-wall carbon nanotubes[53]—to reduced NG. The correspondingly formed charge-transfer state is metastable and decays with a lifetime of 164 ps.

CONCLUSIONS

In conclusion, we have implemented two powerful strategies for interfacing QDs onto the basal plane of graphene in either exfoliated graphite or nanographene to afford QD-pyrene/EG (*i.e.*, direct approach) or QD/pyrene$^+$/NG (*i.e.*, sequential approach), respectively, Figure 11.

We succeeded in avoiding the harsh oxidation steps of graphite to graphene oxide and subsequent chemical reduction to reduced graphene oxide, enabling a fast, cheap, and reproducible way to produce QD-graphene-based hybrid systems. Common to both approaches are pyrenes as multifunctional anchors, whose immobilization onto EG and NG is driven by hydrophobic−hydrophobic and $\pi-\pi$ stacking interactions. QDs were either already covalently linked to pyrene and, in turn, immobilized onto EG in a single step or associated with NG by electrostatic forces in a subsequent second step to avoid aggregation. From full-fledged spectroscopic and microscopic assays we infer that the degree of exfoliation strongly impacts the electronic communication between EG/NG, on one hand, and QDs, on the other hand. To this end, the sequential approach (*i.e.*, QD/pyrene$^+$/NG nanohybrids), where a high degree of exfoliation was achieved prior to the attachment of QDs, is far more superior to the direct approach (*i.e.*, QD-pyrene/EG nanohybrids). As a matter of fact, in the QD/pyrene$^+$/NG nanohybrids a metastable charge-transfer state evolves upon photoexcitation. Aggregation of QDs, which is known to deactivate photoexcited QDs, is, however, ruled out.

In previous work with reduced graphene oxide decorated with CdTe an intensity increase in electrogenerated chemiluminescence of CdTe QDs was seen in the presence of graphene oxide.[54] However, the emission evolves in this particular case by electrogeneration as a recombination of oxidized CdTe and superoxide radical anion. Electron-transfer emission quenching, on the other hand, was reported when reduced graphene oxide was added to a molecular chromophore such as porphyrins. In fact, the latter work reports as well transient absorption measurements that are, however, limited to the 450−750 nm range as a reflection of the porphyrin-centered features.[55] Taking the aforementioned results in combination with our own preliminary experiments on graphene oxide/reduced graphene oxide, a clear optical signature in the form of, for example, a characteristic transient bleach in the near-infrared region is seen to develop only for our nanographene. We believe that this constitutes a major advantage in characterizing energy- and electron-transfer reactions with graphenoid materials.

METHODS

Syntheses and all of the measurements were carried out under an argon atmosphere to prevent oxidation of CdTe QDs. All chemicals used for synthesis were of highest available purity or of analytical grade and were used without further purification.

Synthesis of TGA/MESNA-Costabilized CdTe QDs. CdTe QDs were synthesized following a method described by Schulz-Drost *et al*. Particle growth for 17 h results in ~3 nm diameter QDs, as inferred from optical absorption[56] and HRTEM measurements. First, the QDs were costabilized with thioglycolic acid (TGA) and 2-mercaptoethanesulfonate (MESNA) through binding of their thiol groups. TGA enables the covalent attachment of 1-pyrenemethylamine through EDC/NHS-mediated peptide condensation, while MESNA ensures exclusively the solubility in water (EDC = 1-ethyl-3-(3-dimethylaminopropyl)carbodiimide, NHS = *N*-hydroxysuccinimide). Purification of the crude QDs was performed by precipitation upon addition of ethanol. For optical and microscopic characterization as well as for further treatment, the dry powder was redissolved in Millipore water.

Functionalization of CdTe QDs with Pyrene. A 10 mL (4.367 mg, 0.016 mmol) amount of 1-pyrenemethylamine in 0.1 mM mercaptoethanesulfonic acid (MES) was mixed with 5 mL each of a 19.3 mM solution of EDC and NHS in 0.1 mM MES. NHS was used to extend the activity of EDC during the peptide condensation. In a subsequent step, 5 mL of a TGA/MESNA-capped CdTe QD suspension was gradually added to the mixture until the pH reached 6 and was left stirring for 5 h at room temperature before storing it at 4 °C overnight. The conjugates were then separated from the crude solution by centrifugation at 20000*g* (14.4 k rpm) at 20 °C. The resulting QD-pyrene precipitate was redissolved in 25 mL of Millipore water, giving a Cd^{2+} concentration of 2.6 mM.

Preparation of QD-Pyrene/EG Nanohybrids. A stable suspension of QD-pyrene/EG was generated by diluting 0.5 mL of QD-pyrene (Cd^{2+} = 2.6 mM) with 9.5 mL of Millipore water to which 4 mg of natural graphite was added. The mixture was then vigorously stirred for 3 days in the dark, at room temperature, and under an argon atmosphere. Prior to spectroscopic and microscopic characterization, the sample was stored for 6 h to let the larger unexfoliated graphite flakes precipitate so that the supernatant was free of bulk material.

Preparation of Pyrene$^+$/NG Nanohybrids. Trimethyl(2-oxo-2-pyrene-1-ylethyl)ammonium bromide (pyrene$^+$) (2.0 mg, 0.005 mmol) was dissolved in 10 mL of water, and 4 mg of natural graphite was added. The mixture was ultrasonicated for 40 min and afterward centrifuged for 30 min at 20*g* (500 rpm). Absorption and fluorescence spectra of the yellow-brown supernatant were measured to monitor the evolution of the excimer band. The sample was then centrifuged at 20000*g* (14.4 k rpm) for 60 min to remove unstacked pyrene$^+$. The precipitate was redispersed with a small amount of water to concentrate the hybrid, and the preceding steps were repeated until the excimer band was absent. The resulting dispersion was of weak gray color and was stable for weeks.

Preparation of QD/Pyrene$^+$/NG Nanohybrids. QD/pyrene$^+$/NG nanohybrids were prepared by mixing QDs with unwashed pyrene$^+$/NG. This was necessary, since upon centrifugation no particular information about the amount of pyrene$^+$ was derived. For comparing QD/pyrene$^+$ and QD/pyrene$^+$/NG it was of utmost relevance to have the same pyrene$^+$ concentration (see Figures S8−S11 for specific concentration) to quantify the impact of NG on the optical properties of the QDs.

Optical Characterization. Steady-state absorption spectra were recorded with a Perkin-Elmer Lambda 35. Steady-state emission spectra were recorded with a Fluoromax-P-spectrometer from Horiba Jobin Yvon. Time-correlated single photon counting spectra were taken with a Fluorolog system (Horiba Jobin Yvon). Signal acquisition was gathered by a Hamamatsu MCP photomultiplier (type R3809U-50). The time profiles were recorded at the emission maximum. All samples were measured in a fused quartz glass cuvette with a thickness of 10 mm.

Femtosecond Transient Absorption Spectroscopy. Femtosecond transient absorption spectra were obtained with a Ti:sapphire

laser system CPA-2101 (Clark-MXR, Inc.) in combination with a Helios TAPPS detection unit from Ultrafast Inc. The initial laser excitation wavelength is 775 nm with a pulse width of 150 fs. The used excitation wavelength was 387 nm, which was generated with a SHG crystal. For the generation of the white light a sapphire crystal of adequate thickness was used. The chirp effect between 420 and 770 nm is approximately 350 fs. The detection was carried out with two CCD cameras, each for a specific measuring range. The spectral window is therefore 415 to 770 nm and 770 to 1600 nm. The delay line allows spectral acquisition up to time delays of 8000 ps. All samples were measured in a fused quartz glass cuvette with a thickness of 2 mm. Data acquisition was done with the software HELIOS Visible/nIR (Newport/Ultrafast Systems).

Raman Spectroscopy. Raman measurements were carried out with a LabRAM ARAMIS Raman spectrometer from Horiba Jobin Yvon that was equipped with a confocal microscope and an automated XYZ-table, using laser excitations of 532 and 633 nm. The sample preparation includes drop-casting the hybrids on a Si substrate with a 300 nm oxide layer and rinsing them with water and methanol to remove the excess of unbound pyrene^{+} and QDs.

FT-IR. FT-IR measurements were recorded with a Bruker FT-Alpha with an ATR unit, which made it possible to measure small amounts of purified and dried powder.

Transmission Electron Microscopy. Sample preparation was performed by drop casting and drying the hybrids on holey carbon-coated copper grids. TEM and HRTEM images were recorded with an 80 kV EM 900 from Carl Zeiss AG and with a 300 kV Philips CM 300 UT, respectively.

Conflict of Interest: The authors declare no competing financial interest.

Acknowledgment. We gratefully acknowledge the DFG, ICMM (Interdisciplinary Center for Molecular Materials), the GSMS (Graduate School of Molecular Science), the EAM cluster, the ZMP (Zentralinstitut für neue Materialien und Prozesstechnik), and Dr. Vito Sgobba for financial and intellectual support.

Supporting Information Available: Additional information on the reference systems, titration experiments, and the atomic force microscopy image is provided. This material is available free of charge via the Internet at http://pubs.acs.org.

REFERENCES AND NOTES

1. Geim, A. K. Graphene: Status and Prospects. *Science* **2009**, *324*, 1530–1534.
2. Geim, A. K.; Novoselov, K. S. The Rise of Graphene. *Nat. Mater.* **2007**, *6*, 183–191.
3. Kim, K. S.; Zhao, Y.; Jang, H.; Lee, S. Y.; Kim, J. M.; Kim, K. S.; Ahn, J. H.; Kim, P.; Choi, J. Y.; Hong, B. H. Large-Scale Pattern Growth of Graphene Films for Stretchable Transparent Electrodes. *Nature* **2009**, *457*, 706–710.
4. Reina, A.; Jia, X.; Ho, J.; Nezich, D.; Son, H.; Bulovic, V.; Dresselhaus, M. S.; Kong, J. Large Area, Few-Layer Graphene Films on Arbitrary Substrates by Chemical Vapor Deposition. *Nano Lett.* **2009**, *9*, 30–35.
5. Hernandez, Y.; Nicolosi, V.; Lotya, M.; Blighe, F. M.; Sun, Z.; De, S.; McGovern, I. T.; Holland, B.; Byrne, M.; Gun'Ko, Y. K.; *et al.* High-Yield Production of Graphene by Liquid-Phase Exfoliation of Graphite. *Nat. Nanotechnol.* **2008**, *3*, 563–568.
6. Das, B.; Voggu, R.; Rout, C. S.; Rao, C. N. R. Changes in the Electronic Structure and Properties of Graphene Induced by Molecular Charge-Transfer. *Chem. Commun.* **2008**, *41*, 5155–5157.
7. Dong, X.; Fu, D.; Fang, W.; Shi, Y.; Chen, P.; Li, L.-J. Doping Single-Layer Graphene with Aromatic Molecules. *Small* **2009**, *5*, 1422–1426.
8. Berger, C.; Song, Z.; Li, X.; Wu, X.; Brown, N.; Naud, C.; Mayou, D.; Li, T.; Hass, J.; Marchenkov, A. N.; *et al.* Electronic Confinement and Coherence in Patterned Epitaxial Graphene. *Science* **2006**, *312*, 1191–1196.
9. Dreyer, D. R.; Park, S.; Bielawski, C. W.; Ruoff, R. S. The Chemistry of Graphene Oxide. *Chem. Soc. Rev.* **2010**, *39*, 228–240.
10. Gao, W.; Alemany, L. B.; Ci, L.; Ajayan, P. M. New Insights into the Structure and Reduction of Graphite Oxide. *Nat. Chem.* **2009**, *1*, 403–408.
11. Cai, W.; Piner, R. D.; Stadermann, F. J.; Park, S.; Shaibat, M. A.; Ishii, Y.; Yang, D.; Velamakanni, A.; An, S. J.; Stoller, M.; et al. Synthesis and Solid-State NMR Structural Characterization of (13)C-Labeled Graphite Oxide. *Science* **2008**, *321*, 1815–1817.
12. Englert, J. M.; Röhrl, J.; Schmidt, C. D.; Graupner, R.; Hundhausen, M.; Hauke, F.; Hirsch, A. Soluble Graphene: Generation of Aqueous Graphene Solutions Aided by a Perylenebisimide-Based Bolaamphiphile. *Adv. Mater.* **2009**, *21*, 4265–4269.
13. Malig, J.; Jux, N.; Kiessling, D.; Cid, J. J.; Vázquez, P.; Torres, T.; Guldi, D. M. Towards Tunable Graphene/Phthalocyanine-PPV Hybrid Systems. *Angew. Chem., Int. Ed.* **2011**, *50*, 3561–3565.
14. Rogach, A. L. *Semiconductor Nanocrystal Quantum Dots: Synthesis, Assembly, Spectroscopy and Applications*; Springer: Heidelberg, 2008.
15. Schmid, G. *Nanoparticles: From Theory to Application*; Wiley-VCH: Weinheim, 2010.
16. Rogach, A. L.; Franzl, T.; Klar, T. A.; Feldmann, J.; Gaponik, N.; Lesnyak, V.; Shavel, A.; Eychmüller, A.; Rakovich, Y. P.; Donegan, J. F. Aqueous Synthesis of Thiol-Capped CdTe Nanocrystals: State-of-the-Art. *J. Phys. Chem. C* **2007**, *111*, 14628–14637.
17. Gaponik, N.; Talapin, D. V.; Rogach, A. L.; Hoppe, K.; Shevchenko, E. V.; Kornowski, A.; Eychmüller, A.; Weller, H. Thiol-Capping of CdTe Nanocrystals: An Alternative to Organometallic Synthetic Routes. *J. Phys. Chem. B* **2002**, *106*, 7177–7185.
18. Lu, Z.; Guo, C. X.; Yang, H. B.; Qiao, Y.; Guo, J.; Li, C. M. One-Step Aqueous Synthesis of Graphene−CdTe Quantum Dot-Composed Nanosheet and its Enhanced Photoresponses. *J. Colloid Interface Sci.* **2011**, *353*, 588–592.
19. Guo, C. X.; Yang, H. B.; Sheng, Z. M.; Lu, Z. S.; Song, Q. L.; Li, C. M. Layered Graphene/Quantum Dots for Photovoltaic Devices. *Angew. Chem., Int. Ed.* **2010**, *49*, 3014–3017.
20. Cao, A.; Liu, Z.; Chu, S.; Wu, M.; Ye, Z.; Cai, Z.; Chang, Y.; Wang, S.; Gong, Q.; Liu, Y. A Facile One-Step Method to Produce Graphene-CdS Quantum Dot Nanocomposites as Promising Optoelectronic Materials. *Adv. Mater.* **2009**, *22*, 103–106.
21. Chang, H.; Lv, X.; Zhang, H.; Li, J. Quantum Dots Sensitized Graphene: In Situ Growth and Application in Photoelectrochemical Cells. *Electrochem. Commun.* **2010**, *12*, 483–487.
22. Geng, X.; Niu, L.; Xing, Z.; Song, R.; Liu, G.; Sun, M.; Cheng, G.; Zhong, H.; Liu, Z.; Zhang, Z.; *et al.* Aqueous-Processable Noncovalent Chemically Converted Graphene-Quantum Dot Composites for Flexible and Transparent Optoelectronic Films. *Adv. Mater.* **2009**, *22*, 638–642.
23. Kim, Y.-T.; Hab, J. H.; Hong, B. H.; Kwon, Y.-U. Electrochemical Synthesis of CdSe Quantum-Dot Arrays on a Graphene Basal Plane Using Mesoporous Silica Thin-Film Templates. *Adv. Mater.* **2009**, *22*, 515–518.
24. Bi, H.; Huang, F.; Liang, J.; Xie, X.; Jiang, M. Transparent Conductive Graphene Films Synthesized by Ambient Pressure Chemical Vapor Deposition Used as the Front Electrode of CdTe Solar Cells. *Adv. Mater.* **2011**, *23*, 3202–3206.
25. Li., Q.; Guo, B.; Yu, J.; Ran, J.; Zhang, B.; Yan, H.; Gong, J. R. Highly Efficient Visible-Light-Driven Photocatalytic Hydrogen Production of CdS-Cluster-Decorated Graphene Nanosheets. *J. Am. Chem. Soc.* **2011**, *133*, 10878–10884.
26. Jia, L.; Wang, D.-H.; Huang, Y.-X.; Xu, A.-W.; Yu, H.-Q. Highly Durable N-Doped Graphene/CdS Nanocomposites with Enhanced Photocatalytic Hydrogen Evolution from Water under Visible Light Irradiation. *J. Phys. Chem. C* **2011**, *115*, 11466–11473.
27. Zhiguo, G.; Shuping, Y.; Zaijun, L.; Xiulan, S.; Guangli, W.; Yinjun, F.; Junkang, L. An Ultrasensitive Electrochemical Biosensor for Glucose Using CdTe-CdS Core-Shell Quantum Dot as Ultrafast Electron Transfer Relay between

Graphene-Gold Nanocomposite and Gold Nanoparticle. *Electrochim. Acta* **2011**, *56*, 9162–9167.
28. Sun, S.; Gao, L.; Liu, Y.; Sun, J. Assembly of CdSe Nanoparticles on Graphene for Low-Temperature Fabrication of Quantum Dot Sensitized Solar Cell. *Appl. Phys. Lett.* **2011**, *98*, 093112.
29. Bi, H.; Huang, F.; Liang, J.; Tang, Y.; Lü, X.; Xie, X.; Jiang, M. Large-Scale Preparation of Highly Conductive Three Dimensional Graphene and its Applications in CdTe Solar Cells. *J. Mater. Chem.* **2011**, *21*, 17366–17370.
30. Wang, Y.; Yao, H.-B.; Wang, X.-H.; Yu, S.-H. One-Pot Facile Decoration of CdSe Quantum Dots on Graphene Nanosheets: Novel Graphene-CdSe Nanocomposites with Tunable Fluorescent Properties. *J. Mater. Chem.* **2011**, *21*, 562–566.
31. Zhu, G.; Xu, T.; Lv, T.; Pan, L.; Zhao, Q.; Sun, Z. Graphene-Incorporated Nanocrystalline TiO_2 Films for CdS Quantum Dot-Sensitized Solar Cells. *J. Electroanal. Chem.* **2011**, *650*, 248–251.
32. Kamat, P. V. Graphene-Based Nanoarchitectures. Anchoring Semiconductor and Metal Nanoparticles on a Two-Dimensional Carbon Support. *J. Phys. Chem. Lett.* **2010**, *1*, 520–527.
33. Lightcap, I. V.; Kosel, T. H.; Kamat, P. V. Anchoring Semiconductor and Metal Nanoparticles on a Two-Dimensional Catalyst Mat. Storing and Shuttling Electrons with Reduced Graphene Oxide. *Nano Lett.* **2010**, *10*, 577–583.
34. Scheuermann, G. M.; Rumi, L.; Steurer, P.; Bannwarth, W. Palladium; Mülhaupt, R. Nanoparticles on Graphite Oxide and Its Functionalized Graphene Derivatives as Highly Active Catalysts for the Suzuki-Miyaura Coupling Reaction. *J. Am. Chem. Soc.* **2009**, *131*, 8262–8270.
35. Kou, R.; Shao, Y.; Wang, D.; Engelhard, M. H.; Kwak, J. H.; Wang, J.; Viswanathan, V. V.; Wang, C.; Lin, Y.; Wang, Y.; *et al*. Enhanced Activity and Stability of Pt Catalysts on Functionalized Graphene Sheets for Electrocatalytic Oxygen Reduction. *Electrochem. Commun.* **2009**, *11*, 954–957.
36. Wang, X.; Xu, C.; Zhu, J. W. Graphene-Metal Particle Nanocomposites. *J. Phys. Chem. C* **2008**, *112*, 19841–19845.
37. Muszynski, R.; Seger, B.; Kamat, P. V. Decorating Graphene Sheets with Gold Nanoparticles. *J. Phys. Chem. C* **2008**, *112*, 5263–5266.
38. Hayashi, H.; Lightcap, I. V.; Tsujimoto, M.; Takano, M.; Umeyama, T.; Kamat, P. V.; Imahori, H. Electron Transfer Cascade by Organic/Inorganic Ternary Composites of Porphyrin, Zinc Oxide Nanoparticles, and Reduced Graphene Oxide on a Tin Oxide Electrode that Exhibits Efficient Photocurrent Generation. *J. Am. Chem. Soc.* **2011**, *133*, 7684–7687.
39. Guldi, D. M.; Zilbermann, I.; Anderson, G.; Kotov, N. A.; Tagmatarchis, N.; Prato, M. Versatile Organic (fullerene)−Inorganic (CdTe nanoparticle) Nanoensembles. *J. Am. Chem. Soc.* **2004**, *126*, 14340–14341.
40. Guldi, D. M.; Rahman, G. M.; Sgobba, V.; Kotov, N. A.; Bonifazi, D.; Prato, M. CNT-CdTe Versatile Donor-Acceptor Nanohybrids. *J. Am. Chem. Soc.* **2006**, *128*, 2315–2323.
41. Schulz-Drost, C.; Sgobba, V.; Gerhards, C.; Leubner, S.; Krick Calderon, R. M.; Ruland, A.; Guldi, D. M. Innovative Inorganic-Organic Nanohybrid Materials: Coupling Quantum Dots to Carbon Nanotubes. *Angew. Chem., Int. Ed.* **2010**, *49*, 6425–6429.
42. Leubner, S.; Katsukis, G.; Guldi, D. M. Decorating Polyelectrolyte Wrapped SWNTs with CdTe Quantum Dots for Solar Energy Conversion. *Faraday Discuss.* **2011**, *155*, 253–265.
43. Ferrari, A. C.; Meyer, J. C.; Scardaci, V.; Casiraghi, C.; Lazzeri, M.; Mauri, F.; Piscanec, S.; Jiang, D.; Novoselov, K. S.; Roth, S.; *et al*. Raman Spectrum of Graphene and Graphene Layers. *Phys. Rev. Lett.* **2006**, *97*, 187401.
44. Sanz, M.; Correa-Duarte, M. A.; Liz-Marzan, L. M.; Douhal, A. Femtosecond Dynamics of CdTe Quantum Dots in Water. *J. Photochem. Photobiol. A* **2008**, *196*, 51–58.
45. Guyot-Sionnest, P.; Hines, M. A. Intraband Transitions in Semiconductor Nanocrystals. *Appl. Phys. Lett.* **1998**, *72*, 686–688.
46. Guyot-Sionnest, P.; Shim, M.; Matranga, C.; Hines, M. Intraband Relaxation in CdSe Quantum Dots. *Phys. Rev. B* **1999**, *60*, R2181–R2184.
47. Tomonari, Y.; Murakami, H.; Nakashima, N. Solubilization of Single-Walled Carbon Nanotubes by Using Polycyclic Aromatic Ammonium Amphiphiles in Water-Strategy for the Design of High-Performance Solubilizers. *Chemistry* **2006**, *12*, 4027–34.
48. Ehli, C.; Rahman, G. M. A.; Jux, N.; Balbinot, D.; Paolucci, F.; Marcaccio, M.; Paolucci, D.; Melle-Franco, M.; Zerbetto, F.; *et al*. Interactions in Single Wall Carbon Nanotubes/Pyrene/Porphyrin Nanohybrids. *J. Am. Chem. Soc.* **2006**, *128*, 11222–11231.
49. No indication for any deterioration such as the formation of TeO_2 is gathered.
50. Wang, Z.; Li, J.; Liu, B.; Hu, J.; Yao, X.; Li, J. Chemiluminescence of CdTe Nanocrystals Induced by Direct Chemical Oxidation and its Size-Dependent and Surfactant-Sensitized Effect. *J. Phys. Chem. B* **2005**, *109*, 23304–23311.
51. Liu, M.; Xu, L.; Cheng, W.; Zeng, Y.; Yan, Z. Surface-Modified CdS Quantum Dots as Luminescent Probes for Sulfadiazine Determination. *Spectrochim. Acta Part A* **2008**, *70*, 1198–1202.
52. Interesting is that fact that preliminary transient absorption measurements with graphene oxide under similar conditions lack such features due to lattice defects/dopants that impact phonon mobility and electronic transitions.
53. Herranz, M. A.; Ehli, C.; Campidelli, S.; Gutiérrez, M.; Hug, G. L.; Ohkubo, K.; Fukuzumi, S.; Prato, M.; Martin, N.; Guldi, D. M. Spectroscopic Characterization of Photolytically Generated Radical Ion Pairs in Single-Wall Carbon Nanotubes Bearing Surface-Immobilized Tetrathiafulvalenes. *J. Am. Chem. Soc.* **2008**, *130*, 66–73.
54. Wang, Y.; Lu, L.; Tang, L.; Chang, H.; Li, J. Graphene Oxide Amplified Electrogenerated Chemiluminescence of Quantum Dots and its Selective Sensing for Glutathione from Thiol-Containing Compounds. *Anal. Chem.* **2009**, *81*, 9710–9715.
55. Wojcik, A.; Kamat, P. V. Reduced Graphene Oxide and Porphyrin. An Interactive Affair in 2-D. *ACS Nano* **2010**, *4*, 6697.
56. Yu, W. W.; Qu, L.; Guo, W.; Peng, X. Experimental Determination of the Extinction Coefficient of CdTe, CdSe, and CdS Nanocrystals. *Chem. Mater.* **2003**, *15*, 2854–2860.